AGU ADVANCING EARTH AND SPACE SCIENCES

Earth's Future

RESEARCH ARTICLE
10.1029/2025EF007084

Multi-Indicator Assessment to Assess the Increasing Impacts of Compound Dry and Hot Events on Global Wheat Yield

Jinpeng Hu[1,2,3], Rastislav Skalsky[2], Gangfeng Zhang[1,3], Christian Folberth[2], and Peijun Shi[1,3,4]

[1]State Key Laboratory of Earth Surface Processes and Disaster Risk Reduction (ESPDRR), Beijing, China, [2]Biodiversity and Natural Resources Program (BNR), International Institute for Applied Systems Analysis (IIASA), Laxenburg, Austria, [3]Academy of Disaster Reduction and Emergency Management, Ministry of Emergency Management & Ministry of Education, Beijing Normal University, Beijing, China, [4]Faculty of Arts and Science, Beijing Normal University, Zhuhai, China

Key Points:

- Multi-indicator assessment shows rising compound dry and hot event (CDHE) frequency, duration, and intensity, especially in arid and semiarid wheat-producing regions
- Evapotranspiration and soil moisture indicators (SPEI–SSTI, SSI–SSTI) improve detection of CDHE-related negative yield anomalies in wheat
- Over 70% of wheat-growing areas experience negative yield anomalies when CDHEs account for more than 10% of the growing season

Supporting Information:

Supporting Information may be found in the online version of this article.

Correspondence to:

P. Shi,
spj@bnu.edu.cn

Citation:

Hu, J., Skalsky, R., Zhang, G., Folberth, C., & Shi, P. (2026). Multi-indicator assessment to assess the increasing impacts of compound dry and hot events on global wheat yield. *Earth's Future*, *14*, e2025EF007084. https://doi.org/10.1029/2025EF007084

Received 6 AUG 2025
Accepted 7 MAR 2026

Author Contributions:

Conceptualization: Jinpeng Hu, Rastislav Skalsky, Peijun Shi
Data curation: Jinpeng Hu, Peijun Shi
Formal analysis: Jinpeng Hu, Rastislav Skalsky, Gangfeng Zhang, Christian Folberth, Peijun Shi
Methodology: Jinpeng Hu, Rastislav Skalsky, Gangfeng Zhang, Christian Folberth, Peijun Shi
Visualization: Jinpeng Hu
Writing – original draft: Jinpeng Hu, Rastislav Skalsky, Gangfeng Zhang, Christian Folberth, Peijun Shi
Writing – review & editing: Jinpeng Hu, Rastislav Skalsky, Gangfeng Zhang, Christian Folberth, Peijun Shi

Abstract In a warming climate, the co-occurrence of drought and heat events increasingly threatens the global wheat yield and food security. However, changes in compound dry and hot events (CDHEs) during the global wheat growing season and their impacts on yield remain largely unknown. Using daily ERA5 reanalysis data, multiple drought indicators including the standardized precipitation index, standardized precipitation evapotranspiration index, standardized soil moisture index (SSI), and heat indicators the standardized temperature index and standardized soil temperature index (SSTI), are compared to assess the evolution of CDHEs and their impacts on wheat yield in major wheat-producing regions (1981–2020). The results indicate significant increases in the frequency, duration, and intensity of global CDHEs, with the most pronounced increases experienced in arid and semiarid regions (Eastern Europe, Central Asia, and Turkey). SSI–SSTI was most sensitive to frequency changes, SPEI–SSTI best captured intensity and duration, and SPI–STI provided conservative estimates. These trends reflect regional hydrothermal conditions, land–atmosphere interactions, and agricultural management. When CDHEs account for more than 10% of the growing season, over 70% of wheat areas experienced negative yield anomalies with an average anomaly of −6.3%; Canada, Australia, and Central Asia were severely impacted, whereas highly irrigated regions (e.g., China and India) were less impacted. Indicator combinations incorporating evapotranspiration and soil moisture (SPEI–SSTI, SSI–SSTI) were most strongly correlated with yield anomalies, highlighting their effectiveness for compound stress detection. This study emphasizes the importance of multi-indicator assessments and regional adaptations for developing climate-resilient agricultural strategies.

Plain Language Summary As the climate warms, extreme drought and heat are occurring more often and can overlap during important crop growth stages. When these two stresses occur at the same time, their impact on wheat production can be much more severe than when they occur separately. This study examined how the frequency, intensity, and duration of such combined events, known as compound dry and hot events, changed globally during the wheat growing season from 1981 to 2020, and how they influenced wheat yields. Multiple approaches, including methods that capture both meteorological and soil conditions, were used to evaluate drought and heat conditions. The results indicate that these compound events are becoming more common and intense, especially in drier regions such as Eastern Europe, Central Asia, and parts of Australia. When these events affected more than 10% of the growing season, over 70% of global wheat-growing areas experienced negative yield anomalies, with an average reduction of 6.3%. In contrast, areas with widespread irrigation, such as China and India, were less affected. These findings reveal that combining different measurement approaches improves the ability to detect crop stress and underscore the need for region-specific adaptation strategies to safeguard food production under increasing climate extremes.

1. Introduction

In the context of global warming, the frequency, duration, and intensity of droughts and extreme heat events have increased significantly, posing serious challenges to agricultural system stability (Lesk et al., 2016; Rezaei et al., 2023). The co-occurrence of drought and extreme heat results in compound dry and hot events (CDHEs) (Hao et al., 2022; Zscheischler et al., 2018). Owing to their synergistic amplification and physiological response mechanisms, CDHEs have complex and severe impacts on crop growth and development processes (Lesk &

Anderson, 2021). Consequently, changes in CDHEs have been documented in recent climate change and agricultural impact studies (Afrooz et al., 2023; He et al., 2024; Li, Wang, Li, et al., 2025, Li, Wang, Liu, et al., 2025). Numerous studies have demonstrated that CDHEs have occurred more frequently and intensified in the last few decades across many global regions, leading to negative yield anomalies and significant regional food security and socioeconomic concerns (Cohen et al., 2021; Yin & Slater, 2023). In addition, climate projections indicate that continued global warming will substantially increase the probability and severity of CDHEs, further exacerbating agricultural system vulnerability (He et al., 2024; Mukherjee & Mishra, 2021; Zhang et al., 2023a). Consequently, CDHEs are expected to emerge as major future climate risks to agriculture, necessitating the development of assessment frameworks based on crop physiological responses to support adaptive agricultural management (IPCC, 2021).

Compound dry and hot event identification relies primarily on joint criteria for both drought and extreme heat, typically on the basis of their spatial and temporal concurrence. Previous studies have demonstrated that the choice of drought and temperature indices directly influences CDHE identification outcomes and the ability to characterize agricultural impacts (He et al., 2024; Hosseinzadehtalaei et al., 2024; Wu, Hao, Zhang, et al., 2020). Drought is a complex phenomenon that includes meteorological, hydrological and agricultural types, each with different climate indicators (Dracup et al., 1980; Moradian et al., 2025). For example, meteorological drought is commonly identified using the standardized precipitation index (SPI) or the standardized precipitation evapotranspiration index (SPEI) (Feng et al., 2021), whereas agricultural drought is better captured by indicators such as the standardized soil moisture index (SSI) (Wu et al., 2021). Similarly, extreme heat is typically defined using daily scale indices such as the standardized maximum temperature index (STI) or the soil surface temperature index (SSTI) (Fan et al., 2024). Most current studies adopt a single combination of drought and extreme heat indices, with limited systematic comparisons of differences among their combinations (Fan et al., 2024; Feng et al., 2021). Moreover, existing research has predominantly focused on monthly or seasonal scales, sometimes combining monthly drought indices with daily extreme heat indicators (Geirinhas et al., 2021; Toreti et al., 2019). These approaches often oversimplify event evolution and fail to adequately capture abrupt or cumulative CDHE characteristics (L. Jiang et al., 2025; Shan et al., 2024). This limitation is particularly critical during the crop growing season, when short-term compound events—such as daily extreme heat superimposed with drought—can cause substantial negative yield anomalies (Yang et al., 2025; Zeng et al., 2023). However, current temporal alignment methods frequently lack sufficient temporal resolution for accurate detection of CDHEs. Therefore, fine-scale identification of CDHEs using multiple drought and extreme heat index combinations is strongly needed (Hao & Chen, 2024).

Wheat, one of the world's three major staple crops, is highly sensitive to both drought and extreme heat (Heino et al., 2023; Zampieri et al., 2017). Compound dry and hot events have thus emerged as a significant threat to wheat production stability in many countries (He et al., 2022; Ma et al., 2025). Research indicates that the impact of CDHEs on wheat yield exceeds that of individual drought or extreme heat events, particularly during key phenological stages such as heading and grain filling, where compound stress can cause irreversible negative yield anomalies (T. Jiang et al., 2025; Zhao et al., 2022). However, most existing studies have focused on regional analyses or specific event case studies and lacked a systematic, global-scale multi-indicator analysis of CDHEs (Hao et al., 2018; Mukherjee et al., 2023). Furthermore, uncertainties and sensitivities in yield impact assessments arising from different index pairings remain inadequately addressed (Bevacqua et al., 2022; Zscheischler & Seneviratne, 2017). These gaps underscore the urgent need for a multi-indicator, high-resolution CDHE identification framework.

Thus, ERA5 daily reanalysis data are used to construct six drought−extreme heat index combinations based on three drought indicators and two heat indicators from meteorological and soil perspectives: SPI−STI, SPI−SSTI, SPEI−STI, SPEI−SSTI, SSI−STI, and SSI−SSTI. Using these combinations, we identify CDHEs during the growing season (1981–2020) in major global wheat-producing regions and systematically reveal their spatiotemporal patterns in terms of frequency, duration, and intensity. Using annual gridded wheat yield data (1982–2015), we analyze the relationships between regional CDHE characteristics and yield anomalies and evaluate the explanatory power of different indicator combinations for yield impacts to unravel spatiotemporal patterns of CDHEs and their effects on wheat yields in key global production regions, with implications for climate risk assessment and agricultural adaptation strategy development.

2. Data and Methods

2.1. Data

This study utilized ERA5 reanalysis data, global wheat yield data sets, and wheat cultivation distribution data to identify compound dry–hot events (CDHEs) and analyze yield responses (Table S1 in Supporting Information S1). Meteorological variables, such as daily precipitation, daily maximum air temperature, 0–7 cm soil moisture, and maximum soil temperature at a horizontal resolution of 0.25°, were retrieved from the ECMWF ERA5 daily reanalysis data set (1980–2020) (Hersbach et al., 2023). To ensure spatial consistency with agricultural data sets such as crop yield and crop calendars, all variables were resampled to 0.5° using bilinear interpolation (Agrafiotis, 2014).

Wheat distribution data, such as harvested area estimates for rainfed and irrigated wheat at a 5 arcmin resolution, were sourced from the SPAM2010 global crop distribution data set (Yu et al., 2020). This data set integrates agricultural census records, remote sensing products, geographic information systems, and regression models to represent global cultivation patterns for 42 crops. To differentiate winter and spring wheat-growing areas, we applied the GEOGLAM-BACS mask developed via the G20 Global Agricultural Monitoring Initiative (GEOGLAM) (Becker-Reshef et al., 2022). This data set incorporates crop-type surveys from major producing and exporting countries, enabling refined wheat-type classification (Figure S1 in Supporting Information S1). Sowing and harvest dates were derived from the GGCMI Phase 3 global crop calendar (Jägermeyr, Müller, Minoli, et al., 2021), which synthesizes existing research, remote sensing observations, and crop model simulations to define growing seasons on the basis of water management system (rainfed or irrigated) and ensure that CDHE identification occurs within actual growing periods (Figure S2 in Supporting Information S1).

Wheat yield data were obtained from the GDHY data set (Iizumi & Sakai, 2020), which provides global wheat yield estimates at a 0.5° resolution from 1981 to 2016. This data set combines statistical yearbooks with satellite-based estimates and is widely used in climate–crop studies (Chen & Wang, 2023; Hamed et al., 2021). To ensure consistency and reliability in yield-related analyses, yield-related analyses in this study were restricted to the 1982–2015 period. To improve spatial completeness in regions with yield data gaps, particularly in major wheat-producing zones, we incorporated the GlobalCropYield5min data set (Cao et al., 2025), which provides data with a fine spatial resolution and enhanced coverage. While GDHY served as the primary data source due to its widespread use and compatibility with other 0.5° data sets in this study, GlobalCropYield5min was used to supplement information in areas with data gaps. The two data sets exhibited strong agreement across most major wheat-growing regions (Figure S3 in Supporting Information S1) and were merged using harvest area weights from SPAM to ensure spatial representativeness and consistency of the combined yield records.

To remove the effects of long-term trends imposed by technological advances and management improvements on wheat yields, we applied robust local estimation scatterplot smoothing (RLOESS) to the annual yield time series for each grid cell (Liu et al., 2022; Ye et al., 2015). This approach has been commonly adopted in previous studies, and the influence of the choice of detrending method on the resulting change in yield has been found to be limited (Müller et al., 2017). The percentage yield anomaly (YA) after detrending was calculated by the following equation:

$$\mathrm{YA} = \frac{Y - Y_{\mathrm{trend}}}{Y_{\mathrm{trend}}} \times 100\% \quad (1)$$

where Y is the original yield and where Y_{trend} is the smoothed trend value. This allows for a more accurate assessment of the interannual variability driven by extreme climate conditions.

2.2. Construction of CDHE Indices

In this study, three types of drought indices were used: the SPI, the SPEI, and the Standardized Soil Moisture Index (SSI). SPI and SPEI were derived from daily inputs using a 30-day trailing window. For SPI, the input was the 30-day precipitation accumulation; for SPEI, the input was the 30-day climatic water balance based on precipitation and potential evapotranspiration (PET), with PET estimated by the Hargreaves method (Droogers & Allen, 2002). SPI was standardized by fitting a gamma distribution with a day-specific zero-precipitation probability, whereas SPEI was standardized by fitting a log-logistic distribution to the water-balance samples

without an explicit zero-probability mass. The SSI was computed from the 30-day trailing mean of ERA5 surface soil moisture (0–7 cm) and standardized using the Gringorten plotting-position formula (Gringorten, 1963). For all indices, parameters were estimated per calendar day at each grid cell from the multi-year daily series to account for seasonality; the inverse standard normal transform was then applied to obtain daily z-scores. The distributional choices follow prior assessments showing that these methods reliably characterize the probability distributions of precipitation and soil-moisture anomalies (Stagge et al., 2015; Vicente-Serrano et al., 2010). Previous studies have shown that such daily 30-day SPI/SPEI are highly consistent with their monthly counterparts while better resolving the intra-monthly onset and cessation of dry or wet spells (Shan et al., 2024; Wang et al., 2021). A comparison at representative wheat-growing grid cells (Figure S4 in Supporting Information S1) further confirms that the daily drought and heat indices used here reproduce the timing and magnitude of events seen in monthly indices, while providing finer intra-seasonal variability during the growing season. As an example, the daily SPI was calculated as follows:

$$\mathrm{SP}_{m,i} = \begin{cases} \sum_{j=i-N_d+1}^{i} P_{m,j}, & i \geq N_d \\ \sum_{j=365-N_d+i+1}^{365} P_{m,j} + \sum_{j=i}^{i} P_{m,j}, & i < N_d \end{cases} \tag{2}$$

$$q_i = \frac{Z_i}{M} \tag{3}$$

$$F_i^d(\mathrm{SP}_{m,i}) = \begin{cases} q_i, & SP_{m,i} = 0 \\ q_i + (1 - q_i) \cdot F_i(SP_{m,i}), & SP_{m,i} > 0 \end{cases} \tag{4}$$

$$\mathrm{SPI}_{m,i} = \Phi^{-1}\left(F_i^d(\mathrm{SP}_{m,i})\right) \tag{5}$$

Here, $\mathrm{SP}_{m,i}$ represents the accumulated precipitation on day i in year m over a 30-day window, $P_{m,j}$ represents the daily precipitation, and $N_d = 30$. q_i represents the probability of zero precipitation on day i, with Z_i denoting the number of years with zero precipitation on that day and M denoting the total number of years. $F_i(\mathrm{SP}_{m,i})$ is the cumulative gamma distribution fitted to the nonzero precipitation values, and F_i^d is the full CDF including zeros. The SPI value is finally obtained by applying the inverse standard normal transformation Φ^{-1} to the complete probability value. The procedures for calculating the SPEI and SSI are detailed in Text S1 in Supporting Information S1.

The extreme heat indices included the standardized maximum temperature index (STI) and the soil surface temperature index (SSTI). Standardized temperature index and SSTI were computed from the 3-day trailing mean of daily maximum 2-m air temperature and soil surface temperature (0–7 cm), respectively, and then standardized using the Gringorten plotting-position method. Parameters were estimated per calendar day at each grid cell to accommodate seasonality, and the standardization emphasizes tail behavior commonly targeted in extreme-climate analyses (Liu & Sun, 2020). Full implementation details are provided in Text S2 in Supporting Information S1. The five indices (SPI, SPEI, SSI, STI, SSTI) are summarized in Table S2 in Supporting Information S1.

On the basis of these indices, six combinations were constructed for multidimensional CDHE identification: SPI–STI, SPI–SSTI, SPEI–STI, SPEI–SSTI, SSI–STI, and SSI–SSTI. A compound dry and hot day was defined as a day with a drought index below −0.8 and a temperature index above 1.3. These thresholds were adapted from earlier studies (Mukherjee & Mishra, 2021; Wang et al., 2023), where similar percentile-based criteria (e.g., 20th percentile for drought and 90th percentile for temperature) were shown to effectively capture the co-occurrence of drought and heat extremes. To validate their suitability for global wheat systems, we conducted a sensitivity analysis by perturbing the drought and heat thresholds within ±0.1–0.2 of −0.8 and 1.3 and evaluating the resulting CDHE occurrence rates and their relationships with yield anomalies in wheat-growing regions. As summarized in Table S3 in Supporting Information S1, the selected thresholds produce occurrence rates consistent with the intended percentile-based intensity, while the negative association between CDHE characteristics and yield anomalies remains stable across these neighboring thresholds, confirming their agricultural relevance and spatiotemporal robustness. Together, the six pairings span precipitation-based, evapotranspiration-

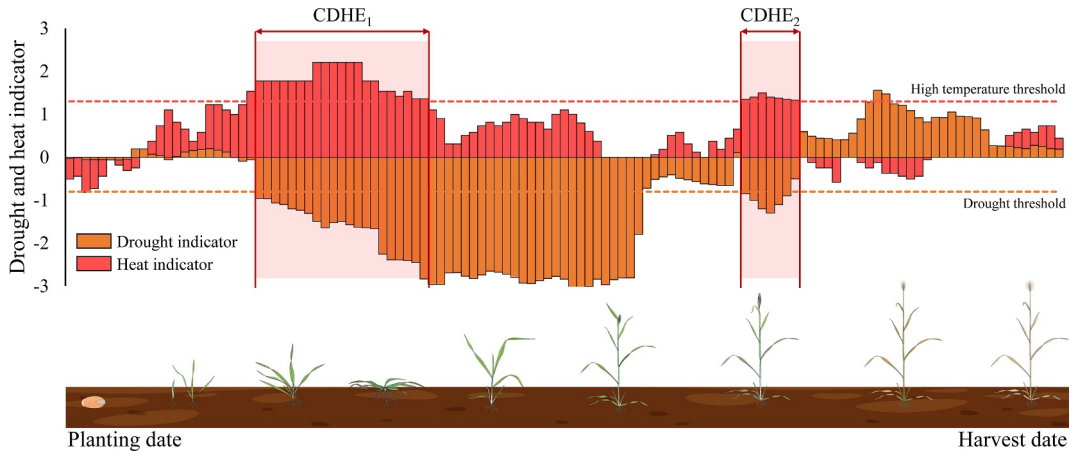

Figure 1. Schematic for the identification of compound dry and hot events throughout the wheat growing season.

based, and soil-moisture-based drought representations, combined with air and land-surface heat metrics, enabling a comparative assessment of how physical representations shape CDHE identification and agricultural relevance.

2.3. Identification and Characterization of CDHE

CDHEs were identified on a daily scale as either consecutive or isolated compound dry and extreme heat days, restricted to the wheat growing season (from planting to harvest) for each grid cell (Figure 1). During each growing season, the number of days with CDHEs was determined on the basis of predefined thresholds, and three annual characteristics were calculated: frequency, duration, and intensity (Table S4 in Supporting Information S1) (Liu et al., 2025).

Frequency was defined as the proportion of CDHEs days to the total number of days in the growing season. Duration was measured as the average number of consecutive days across all CDHEs in a given year. According to previous studies (Gu et al., 2022; Wu et al., 2019), the intensity of compound extreme events can be described using functional relationships between event-level drought and heat characteristics. In this study, CDHE intensity was defined as the cumulative sum of the products of drought and heat index values across all CDHE days within each event. The annual average intensity per event was used as the representative intensity metric. These statistical methods are as follows:

$$F_{i,g} = \frac{N_{i,y}^{\mathrm{CDHE}}}{N_{i,y}^{GS}} \times 100\% \tag{6}$$

$$D_{i,g} = \frac{1}{n_{i,y}} \sum_{j=1}^{n_{i,y}} L_{i,y}^{(j)} \tag{7}$$

$$I_{i,g} = \frac{1}{n_{i,y}} \sum_{j=1}^{n_{i,y}} \sum_{t \in \mathrm{event}_j} |D_{i,t}| \times T_{i,t} \tag{8}$$

where i denotes the spatial grid cell, and y denotes the calendar year; $N_{i,y}^{\mathrm{CDHE}}$ is the number of CDHE days in the growing season; $N_{i,y}^{\mathrm{GS}}$ is the total number of days in the growing season; and $n_{i,y}$ is the number of discrete CDHEs in that season. $L_{i,y}^{(j)}$ is the duration (in days) of the jth CDHE, and $D_{i,t}$ and $T_{i,t}$ are the standardized drought and temperature index values on day t for a given event.

All CDHE characteristics, namely, frequency, duration, and intensity, were first calculated at the grid-cell level during the wheat growing season. To obtain representative values for each grid cell, CDHE metrics were integrated across rainfed and irrigated systems for both winter and spring wheat (Figure S5 in Supporting

Information S1), using the respective harvested areas as weights. This approach ensured that both crop type and water management differences were accounted for in the weighted averages. The resulting integrated values were then used to support subsequent analyses of wheat yield responses and regional sensitivity.

$$V_i^{\text{winter}} = \frac{A_i^{\text{irr}} \cdot V_i^{\text{winter,irr}} + A_i^{rf} \cdot V_i^{\text{winter,rf}}}{A_i^{irr} + A_i^{rf}} \tag{9}$$

$$V_i^{\text{spring}} = \frac{A_i^{\text{irr}} \cdot V_i^{\text{spring,irr}} + A_i^{\text{rf}} \cdot V_i^{\text{spring,rf}}}{A_i^{irr} + A_i^{rf}} \tag{10}$$

$$V_i^{\text{wheat}} = \frac{A_i^{\text{winter}} \cdot V_i^{\text{winter}} + A_i^{\text{spring}} \cdot V_i^{\text{spring}}}{A_i^{\text{winter}} + A_i^{\text{spring}}} \tag{11}$$

where V_i^{wheat} denotes the final area-weighted value (frequency, duration, or intensity) for the grid cell. A represents the harvested area; the superscripts "winter" and "spring" refer to seasonal wheat types, and the subscripts "irr" and "rf" denote irrigated and rainfed systems, respectively.

To verify that the six CDHE definitions represented comparable event characteristics, we applied non-parametric Friedman tests followed by pairwise comparisons with Benjamini–Hochberg false discovery rate (FDR) correction (Benjamini & Hochberg, 1995; Friedman, 1937). This procedure ensured that the multi-index framework yielded robust and internally consistent CDHE characterizations.

2.4. Assessment of the CDHE-Yield Relationship

On the basis of detrended YA data, the Pearson correlation coefficients (Pearson, 1895) between CDHE statistical characteristics (frequency, duration and intensity) and wheat yield anomalies were calculated across six combinations of drought and heat indices. The analysis was conducted at the global scale and further aggregated to the national level to identify regional differences and response sensitivities. Eleven major wheat-producing countries (Figure S6 in Supporting Information S1), which together account for more than 70% of global wheat production (data from FAOSTAT), were selected for this analysis. Correlation analysis was used to identify the most representative index combinations and CDHE construction methods, which were then applied to assess yield responses at the global and national scales. For each grid cell i and year y, the correlation was calculated using the following formula:

$$r_i = \frac{\sum_{y=1}^{n}\left(V_{i,y} - \overline{V_i}\right)\left(Y_{i,y} - \overline{Y_i}\right)}{\sqrt{\sum_{y=1}^{n}\left(V_{i,y} - \overline{V_i}\right)^2}\sqrt{\sum_{y=1}^{n}\left(Y_{i,y} - \overline{Y_i}\right)^2}} \tag{12}$$

where $V_{i,y}$ is the CDHE characteristic (frequency, duration, or intensity) in grid cell i for year y, and $Y_{i,y}$ is the detrended wheat YA. $\overline{V_i}$ and $\overline{Y_i}$ represent the multiyear means of the respective variables.

To further evaluate yield responses under different compound-event exposures, grid–year data were grouped according to the proportion of CDHE days during the growing season (<10%, 10%–20%, 20%–30%, and ≥30%) for each indicator combination. The corresponding yield anomalies (%) for each exposure level were summarized as boxplots representing the interquartile distribution. Statistical differences in yield anomalies across CDHE frequency levels were assessed to identify significant negative yield anomalies under higher exposure.

3. Results

3.1. Changes in of CDHE Characteristics During the Global Wheat Growing Season

During 1981 and 2020, CDHEs occurred widely across global wheat-growing regions, exhibiting pronounced spatial variability and a clear increasing trend (Figures 2–3). On average, 3.63% of the days during the wheat growing season were affected by CDHEs. Exposure was significantly greater in midlatitude continental regions, such as the midwestern United States, the Eastern Europe−West Asia grain belt, Central Asia, and the North China Plain, than in other regions. In the Southern Hemisphere, regions of Argentina and Australia exhibited

10.1029/2025EF007084

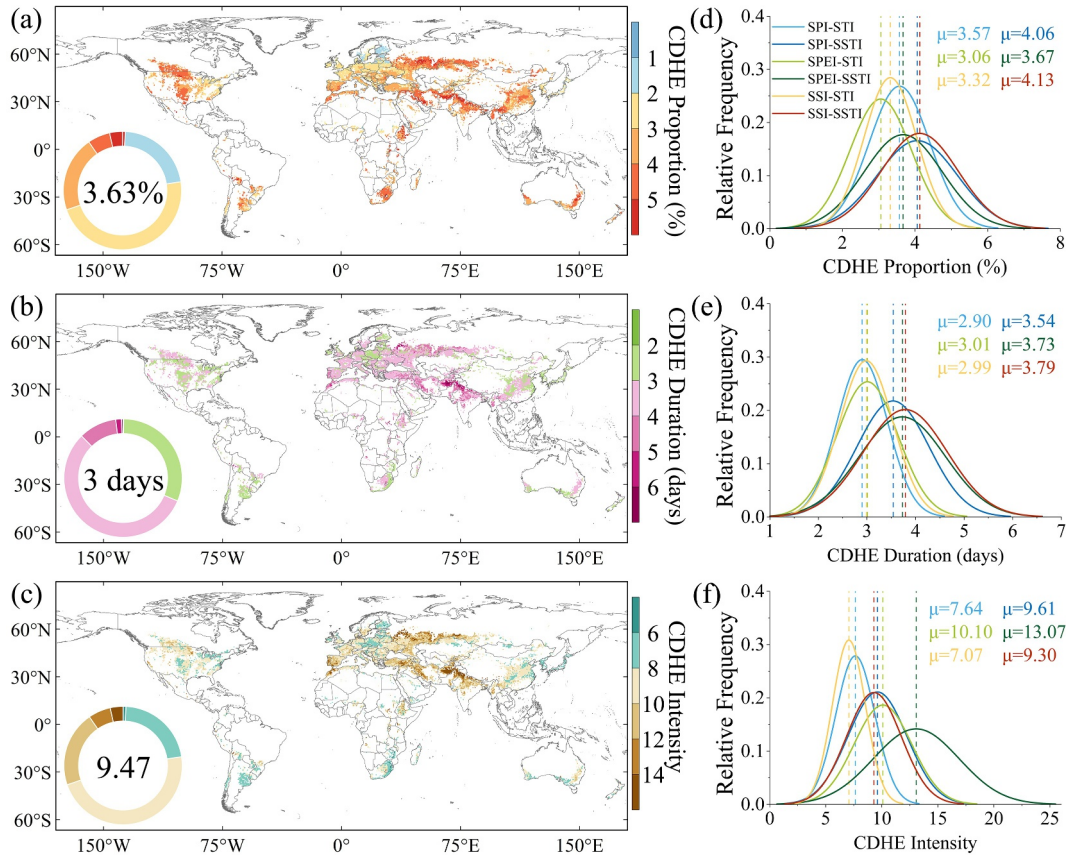

Figure 2. Spatiotemporal characteristics of compound dry and hot events (CDHEs) in global wheat-growing regions from 1981 to 2020. (a)–(c) Multi-index averages of CDHE characteristics: (a) proportion of CDHE days during the wheat growing season, (b) average event duration (days), and (c) average event intensity. (d)–(f) Relative frequency distributions of (d) the proportion of CDHE days, (e) event duration, and (f) event intensity across six drought–temperature index combinations: SPI–STI, SPI–SSTI, SPEI–STI, SPEI–SSTI, SSI–STI, and SSI–SSTI.

higher-than-average CDHE exposure compared with other wheat-growing regions (Figure 2a). In contrast, humid regions such as Western Europe exhibited lower proportions of CDHE days, indicating that the global CDHEs are more concentrated in hotter, drier regions, posing a significant threat to wheat production systems.

The average duration of a CDHE globally was approximately 3 days (Figure 2b). However, in regions such as South Asia and West Asia, individual events frequently persisted for over 4–5 days. In contrast, most CDHEs in temperate humid regions end within 2–3 days. The spatial distribution of CDHE intensity (Figure 2c) revealed a distinct regional cluster, for example, Central Asia, Eastern Europe, and southern Siberia presented mean intensity values exceeding the global average (9.47). This pattern suggests more pronounced synergistic effects between drought and extreme heat in these regions.

Substantial differences in CDHE characteristics were observed among the six drought–temperature index combinations (Figures 2d–2f). In terms of frequency, combinations with the SSTI, particularly the SPI−SSTI and SSI−SSTI combinations, detected a greater proportion of CDHE days. In contrast, STI-based combinations more often captured short-lived, spatially dispersed heat extremes, yielding lower accumulated frequencies. Cross-definition differences were statistically significant, with overall differences detected among the six definitions for each metric ($p < 0.05$). After pairwise comparison and FDR adjustment, frequency differences were mainly associated with the drought index (SPI, SPEI, SSI), whereas duration and intensity were predominantly driven by the heat metric (SSTI > STI) (Figure S7 in Supporting Information S1).

Different indicators exhibit varying sensitivities in capturing drought and heat events, and the choice of indicators has a significant effect on the identification of CDHE characteristics (Figures S8 and S9 in Supporting

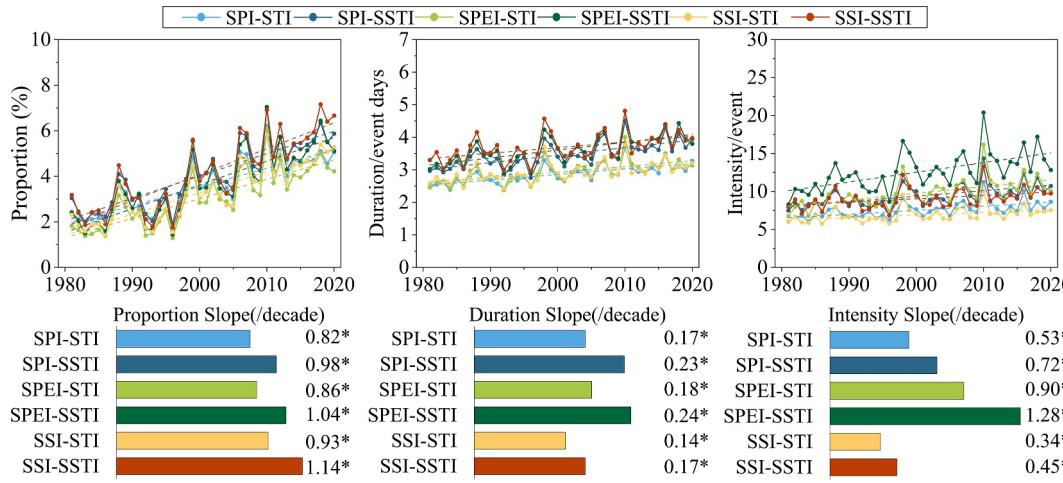

Figure 3. Variability in compound dry and hot event (CDHE) characteristics in global wheat-producing regions from 1981 to 2020. (proportion: percentage of CDHE days relative to the total number of growing-season days; duration: average number of days per CDHE event; intensity: average intensity per event calculated as the accumulated product of daily standardized drought and heat index values). Note: The bars below each panel represent the decadal trends (slopes) of the corresponding CDHE metrics, and asterisks (*) denote statistically significant trends ($p < 0.05$).

Information S1). Overall, the SPI (meteorological precipitation index) is more sensitive to short-term precipitation anomalies, such as the higher average CDHE frequency for the identification of SPI−STI combinations ($\mu = 3.57\%$), whereas the SPEI (consideration of evapotranspiration equilibrium) is more strictly defined with a lower average frequency of dry heat ($\mu = 3.06\%$) (Figure 2d). The standardized soil moisture index (SSI), characterized by its ability to represent long-term drought conditions, presented the highest average frequency of detection of CDHEs when it is combined with the SSTI ($\mu = 4.13\%$) (Figures 2d–2f). These contrasts align with soil-moisture memory (SSI carries antecedent deficits) and reduced evaporative cooling over dry soils (captured by SSTI), which together favor more persistent dry–hot co-occurrence. The higher exposure under SSI–SSTI is consistent with the single-hazard diagnostics (Figure S8 in Supporting Information S1).

Regarding duration, combinations using SSTI event definitions were more focused on continuity (Figure 2e), with longer average durations (e.g., SSI−SSTI: $\mu = 3.79$ days). In contrast, SPI–STI combinations identified shorter events ($\mu = 2.90$ days; Figure 2e). Differences in intensity were particularly pronounced, with the SPEI−SSTI combination identifying the highest event intensity ($\mu = 13.07$), whereas combinations such as SPI−STI and SSI−STI were on the lower side ($\mu = 7.64$ and $\mu = 7.07$, respectively; Figure 2f). This indicates that the evapotranspiration factor considered by the SPEI amplifies the synergistic effect of drought and heat, whereas the SPI and SSI have relatively low intensities under the definition of a single meteorological or soil variable (Figure S8 in Supporting Information S1).

From 1981 to 2020 (Figure 3), CDHE frequency, duration, and intensity increased significantly. Across the six definitions, average trends were 0.82%–1.14% decade^{-1} for frequency, 0.14–0.24 days decade^{-1} for duration, and 0.34–1.28 units decade^{-1} for intensity. SSTI-based combinations generally showed greater increases, suggesting that soil heat anomalies exert a stronger influence on CDHE trends. SPEI-related combinations were the most sensitive for intensity, with SPEI–SSTI showing the greatest increase (1.28 units decade^{-1}), whereas SSI-based combinations exhibited relatively weaker intensity trends but more pronounced increases in frequency. For intensity, the cross-definition differences in trend slopes are statistically significant ($p < 0.05$, ANCOVA), supporting the interpretation that different drought–heat representations lead to different rates of long-term CDHE intensification.

3.2. Characteristics of CDHE During the Wheat Growing Season in Major Producing Countries

The 11 major wheat-producing countries worldwide show consistent intensification and significant regional heterogeneity in the exposure levels and trends of CDHEs (Figure 4). The results suggest that, in a warming

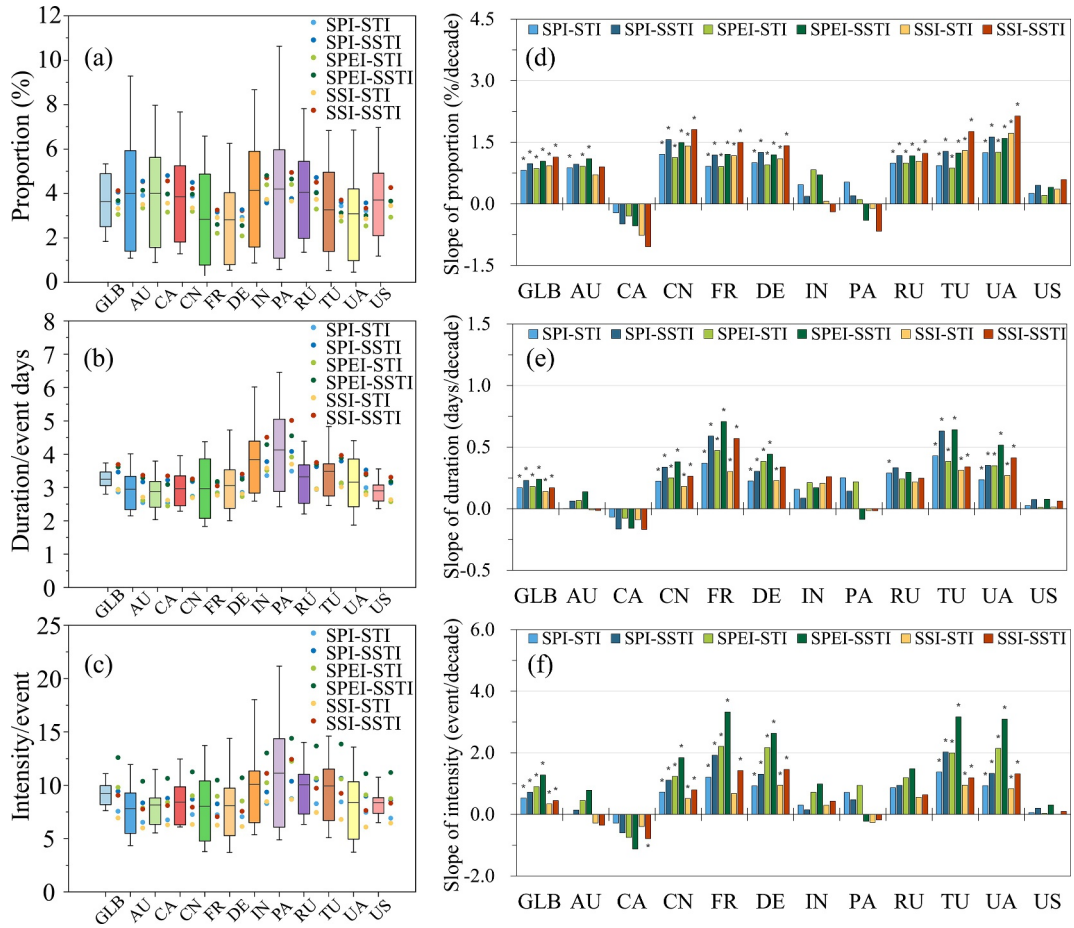

Figure 4. Compound dry and hot event (CDHE) characteristics and trends in 11 major wheat-producing countries during the growing season (1981–2020). (a–c) Average proportion of CDHE days, duration, and intensity by country and index combination. (d–f) Corresponding linear trends (per decade). Note: (AU: Australia, CA: Canada, CN: China, FR: France, DE: Germany, IN: India, PA: Pakistan, RU: Russia, TU: Turkey, UA: Ukraine, US: United States)

climate, the main wheat-producing countries generally face higher frequency, stronger intensity and longer duration of the compound dry heat risk (Figure S10 in Supporting Information S1).

Overall (Figures 4a–4c), there are clear regional differences in CDHE characteristics across the main producing countries. The proportion of CDHE days within the growing season was highest in Pakistan (3.66%–4.94%) and India (3.57%–4.81%), indicating severe CDHE exposure in South Asia. In contrast, the United States, China, and Australia had medium to high percentages (2.97%–4.8%) of CDHE days, and France, Germany, and other European countries generally had lower percentages (2.21%–3.27%) of proportion of CDHE days.

For duration, Pakistan had the longest average CDHE duration (3.49–5.01 days), followed by India (3.36–4.51 days), whereas North American countries (Canada and the United States) and Australia had relatively shorter durations (2.54−3.36 days). Combinations that use the SSTI as the heat index tended to display longer durations than those using the STI. For example, in Pakistan, the SPEI–SSTI combination had an average duration of 5.01 days, whereas the average duration of SPI–STI was 3.49 days. Regarding intensity, Pakistan and India had the highest CDHE intensities, with those of SPEI–SSTI combination reaching 14.39 and 13.02, respectively, followed by Russia, Turkey, and China, whereas Canada and Australia presented lower intensity values (5.99–10.64). Mechanistically, SSTI reflects near-surface soil heat accumulation and reduced evaporative cooling under dry soils, favoring longer and stronger events; pairing with SPEI amplifies this response via the water-balance (PET) signal. These cross-definition contrasts were statistically supported, with overall distributional differences (Friedman $p < 0.05$) and most pairwise comparisons remaining significant after multiple-comparison correction (Figure S7 in Supporting Information S1).

10.1029/2025EF007084

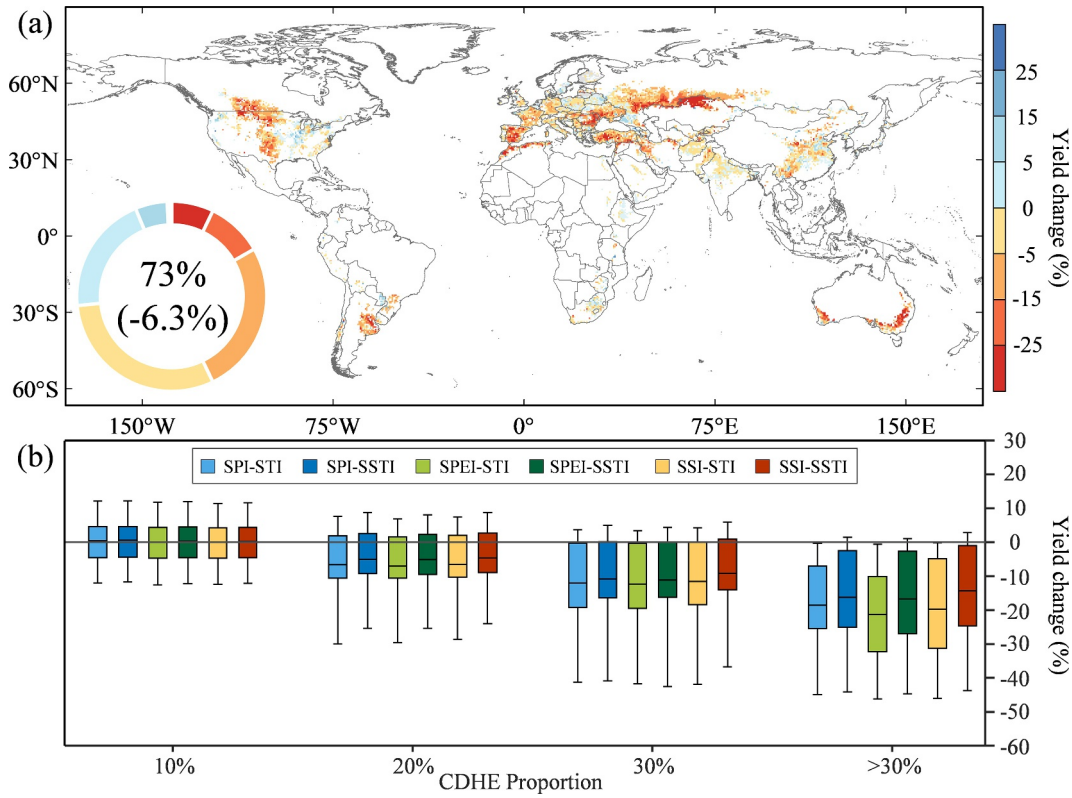

Figure 5. Relationship between the frequency of compound dry and hot events (CDHEs) and wheat yield changes. (a) Spatial distribution of yield anomalies in response to high CDHE frequencies (>10%) across global wheat-growing regions. (b) Yield changes for different CDHE frequency intervals and drought–temperature index combinations.

The frequency, duration, and intensity of CDHEs significantly increased across most major producing countries from 1981 to 2020, but the magnitude and significance of the trends differed significantly among countries (Figures 4d–4f). With respect to the frequency of CDHEs, China, Ukraine, and Turkey showed the most significant increases (0.87%–2.14% decade^{-1}), whereas Canada and Pakistan showed flat or slightly decreasing trends. The increase in event duration was more prominent in France (a maximum of 0.71 days decade^{-1}) and Turkey (a maximum of 0.64 days decade^{-1}), whereas Canada and Australia showed insignificant changes in CDHE duration. The increase in event intensity was most evident in France (maximum of 3.32 units per decade), Germany, Ukraine, and Turkey. In contrast, the event intensities in Canada and Australia experienced slight declines or were stable.

The sensitivity of different combinations of indicators to trend estimation varied. Combinations involving the SSTI generally detected stronger increases in frequency, duration, and intensity—particularly in China, France, Germany, Turkey, and Ukraine. SPEI-based combinations were more responsive in capturing the intensification of CDHE severity, consistent with water-balance anomalies that are amplified under hot–dry conditions (higher PET), thereby steepening intensity trends. In contrast, SSI-based trends were comparatively moderate, as soil moisture integrates and lags atmospheric forcing, thereby dampening short-term intensification signals.

3.3. Relationship Between CDHEs and Wheat Yield Changes

When the frequency of CDHEs exceeded 10%, approximately 73% of the global wheat-growing regions experienced negative yield anomalies, with a mean anomaly of −6.3% (Figure 5a). The areas with negative yield anomalies were mainly distributed from Eastern Europe to the West Asia Grain Belt, central North America, southern South America, and southeastern Australia, which are areas with a high frequency of CDHEs, indicating significant spatial aggregation. This suggests that when the frequency of the CDHE exceeds the critical threshold,

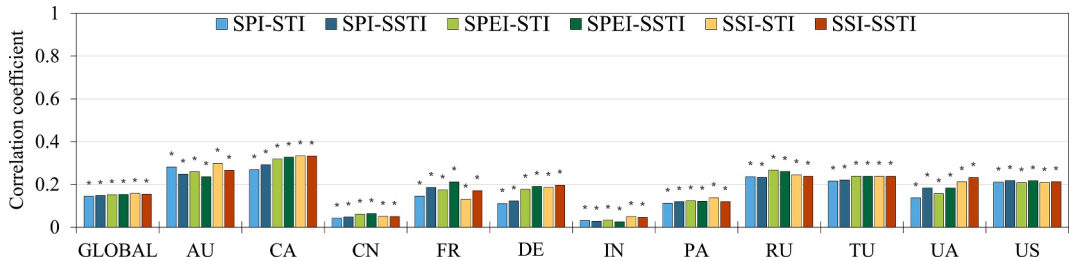

Figure 6. Correlation between the proportion of compound dry and hot events and wheat yield anomalies. Note: Each country's correlation was computed using all valid wheat grid–year observations (sample size = number of grid cells × number of years). Asterisks indicate statistically significant correlations ($p < 0.05$).

the global wheat production in the main producing regions is systematically suppressed, and the areas with increases in production are limited in size and scattered.

Further analysis revealed the distribution of the wheat yield response with respect to the percentage of occurrence of CDHE under different combinations of drought and high-temperature indicators (Figure 5b). Overall, as the percentage of dry−heat events increased from 10% to >30%, the negative yield anomalies significantly increased for all indicator combinations. When the frequency of occurrence was above 30%, the SPEI–STI combination resulted in the greatest mean negative YA (−21.22%), followed by SSI–STI (−19.57%) and SPI–STI (−18.48%), whereas the SSI-SSTI combination resulted in the smallest anomaly (−14.18%). The combinations that use the STI as a temperature indicator were generally more sensitive for identifying yield declines than the SSTI was for the same drought indicator. Although the distribution of yield changes characterized by each group of indicators was similar, the magnitude of yield changes reflected sensitivity differences. Drought indices incorporating evapotranspiration or soil moisture components, such as the SPEI and SSI, exhibited greater sensitivity and consistency in explaining negative yield anomalies under high-frequency CDHE conditions.

A conditional probability analysis at the annual scale revealed a pronounced amplification of yield-anomaly risk associated with CDHEs (Figure S11a in Supporting Information S1). The likelihood of negative yield anomalies in CDHE years (0.67) exceeds that in years with individual drought or heat extremes by roughly one-third. This elevated risk is compounded by a substantially greater mean negative YA during CDHEs compared to single-hazard events (Figure S11b in Supporting Information S1), highlighting a synergistic impact that leads to disproportionately large losses.

To further quantify the statistical relationship between the frequency of CDHEs and wheat yield anomalies, Figure 6 presents the correlation coefficients between the six indicator combinations and wheat yield at the global and national scales. At the global level, the correlations between all indicator combinations and negative yield anomalies loss are positive (0.14−0.16), indicating that an increase in the frequency of CDHEs consistently decreases the wheat yield in the main producing regions of the globe overall, regardless of the type of drought−high temperature indicator used. The narrow range of correlations mainly reflects spatial averaging across diverse agro-climatic environments, and thus the overall sign and magnitude of correlations appear robust to index choice at the global scale, while regional performance may still vary depending on hydroclimatic context and water-management conditions.

At the national scale, wheat yield responses to CDHE frequency exhibit greater variability (Figure S12 in Supporting Information S1). Canada has the greatest sensitivity, with correlation coefficients reaching 0.33 for the SSI–STI, SSI–SSTI, and SPEI–SSTI combinations, the highest among those of all countries. Australia follows closely (0.25–0.30), whereas Russia, Turkey, Ukraine, and the United States exhibit moderate to strong correlations (0.21–0.27). The correlations for France, Germany, and Pakistan are relatively weak (0.11–0.21). In contrast, all index combinations in China and India exhibit extremely low correlations (<0.07). This does not necessarily indicate that CDHEs have no impact in these regions. It may instead suggest that their direct effects on yield may be significantly buffered by widespread irrigation coverage, or that the underlying impact mechanisms are more complex and not fully captured by the selected indices.

In the comparison of indicator combinations, the combination of the SSI and SSTI performs best in drought and high temperature risk regions such as Canada and Australia, indicating that soil water deficit in the root zone and

persistent heat stress have a stronger control on wheat yield. In Russia, Western Europe and other middle and high-latitude regions, the SPEI-STI combination and other weather–evapotranspiration indicators better reflect the compound effect of high temperatures superimposed with drought and have stronger explanatory power for yield changes; while SPI combinations are effective in some regions, their overall stability and response strength are weaker. The low correlations observed in China and India further suggest that the direct effect of CDHE on yield is relatively limited in areas with extensive irrigation coverage. Taken together, these patterns indicate that global-scale robustness does not preclude regional differentiation, and that index selection should reflect dominant stress pathways and local water management. Overall, the relatively consistent correlations across index combinations suggest that index choice does not materially alter the global-level conclusion; however, it remains important for regional or process-oriented analyses, where representations of evapotranspiration or soil-moisture dynamics (e.g., in SPEI- or SSI-based definitions, especially with SSTI) can better capture yield sensitivity to CDHEs.

4. Discussion

4.1. Attribution Analysis of Spatiotemporal Patterns and Regional Response Mechanisms

Changes in CDHE characteristics are closely related to global warming (Goulart et al., 2021; Hu et al., 2024). This study revealed that between 1981 and 2020, there was a strong correlation between temperature during the growing season in global wheat-growing regions and changes in CDHE characteristics. As temperatures rose during the growing season, the frequency, duration, and intensity of CDHEs tended to increase (Figure S13 in Supporting Information S1). Rising temperatures increase potential evapotranspiration (PET), exacerbating soil moisture deficits under conditions of insufficient precipitation and thereby increasing the probability of concurrent drought and heat events (Gebrechorkos et al., 2025). A critical process driving this phenomenon is the land–atmosphere coupled feedback mechanism. Drought conditions reduce the cooling effect associated with vegetation evapotranspiration, increasing surface sensible heat fluxes. This process, in turn, elevates surface and air temperatures, establishing a positive feedback loop whereby drought and heat mutually reinforce each other (Heino et al., 2023). The 40-year period analyzed in this study is sufficient to capture robust multidecadal tendencies in CDHE frequency, duration, and intensity. Nevertheless, these variations likely reflect the combined influence of externally forced climate change and internal climate variability. The observed long-term trends are consistent with the expected response to anthropogenic greenhouse-gas forcing, while part of the regional and interdecadal fluctuations may be associated with large-scale natural variability modes such as the Pacific Decadal Oscillation (PDO) and the Atlantic Multidecadal Oscillation (AMO) (Lin & Qian, 2022; McKinnon & Deser, 2018; Newman et al., 2016).

At the regional scale, the variation in CDHE characteristics exhibited significant spatial heterogeneity. These regional differences are not only related to hydrothermal conditions, but also closely related to local land–atmosphere interactions and agricultural management practices (Hao et al., 2022; Tripathy et al., 2023). In arid and semiarid regions (e.g., parts of Central Asia, West Asia, and South Asia), limited background soil water storage leads to rapid soil moisture depletion during precipitation deficits, which increases the intensity and persistence of surface temperature responses. As a result, CDHEs in these areas tend to be more intense and prolonged (Figure S14 in Supporting Information S1). South Asia, which depends highly on monsoonal rainfall, is particularly vulnerable to the rapid co-occurrence of drought and heat due to monsoon variability (Rajeev et al., 2022). Notably, even humid regions such as France and Germany have experienced a marked increase in the number of CDHEs in recent years, driven by reduced summer precipitation and more frequent heatwaves (Markonis et al., 2021). This suggests that under ongoing climate warming, humid regions are also increasingly exposed to CDHE risk. In contrast, wheat-producing regions in North America (e.g., the United States and Canada) exhibit relatively weak or non-significant trends in CDHE frequency and intensity. Analysis of growing-season temperature trends revealed that these regions experienced relatively modest warming compared to other major production areas (Figure S15 in Supporting Information S1), suggesting that a lower rate of warming may limit the exacerbation of CDHEs (He et al., 2024).

4.2. Impact of Indicator Selection on CDHE Identification and Applicability Assessment

Different combinations of drought and temperature indicators exhibit marked differences in their ability to identify CDHE characteristics, reflecting inherent differences in their physical interpretations and responsiveness

to dry–heat processes (Afrooz et al., 2023). The SPEI, which incorporates the impact of temperature on evapotranspiration, is more sensitive for capturing the synergistic intensification of dry–heat stress (Peng et al., 2024). When combined with the SSTI, the SPEI–SSTI pairing typically identifies the highest CDHE intensity and rates of increase, which is particularly notable in regions such as China, South Asia, and Eastern Europe. In contrast, the SPI, which accounts for only precipitation anomalies, is more sensitive to short-term rainfall variability and is less capable of capturing prolonged drought–heat interactions. The standardized soil moisture index (SSI), on the other hand, reflects the soil water content with inherent lag and buffering effects, often delaying the detection of drought signals. Consequently, CDHE trends identified using SPI or SSI-based combinations tend to be more conservative (Feng et al., 2021; Prabhakar et al., 2023).

The choice of high-temperature indicators is also critical. The STI reflects near-surface air temperature anomalies and is more sensitive to short-lived heatwaves, whereas the SSTI is based on soil temperature and exhibits stronger thermal inertia and cumulative effects, making it more suitable for identifying longer-lasting heat anomalies. When SSTI is combined with SSI, the resulting CDHE definitions directly couple root-zone soil-moisture deficits with elevated soil temperatures, characterizing episodes when soils are both dry and anomalously warm. In rain-fed systems, pairing SSTI with SPEI provides a complementary view of atmospheric water-balance stress that often coincides with progressive drying of the root zone. Under such coupled water–heat stress, elevated soil temperatures and low soil moisture can constrain root growth, reduce root hydraulic conductance, and limit water and nutrient uptake along the soil–plant–atmosphere continuum, thereby increasing the vulnerability of yield formation to CDHEs (Fahad et al., 2017; Tricker et al., 2018). Recent evidence that soil heat extremes can outpace air temperature extremes (García-García et al., 2023) further supports the use of soil-temperature-based indices such as SSTI to represent the persistent thermal component of CDHEs that directly affects crop root systems. Accordingly, SSTI-related combinations (such as SPEI–SSTI and SSI–SSTI) typically identify CDHEs with higher frequencies, longer durations, and stronger trends, and show tighter links to negative yield anomalies in drought- and heat-prone regions (Fan et al., 2024). This also indicates that the SPEI–SSTI and SSI–SSTI combinations can serve as observational benchmarks for evaluating whether climate and Earth System Models (e.g., CMIP6) realistically reproduce soil-moisture–temperature coupling and agriculturally relevant compound dry–hot extremes.

Overall, the contrast among these indicators underscores the importance of selecting physically meaningful indices that align with regional climate characteristics and agricultural management needs in CDHE risk assessment. For example, in semi-arid regions, combinations such as SSI–SSTI or SPEI–SSTI are more effective at capturing root-zone water–heat stress interactions (Zhang et al., 2023b), whereas in humid regions where droughts are mainly precipitation-driven, the SPI–STI combination remains applicable.

4.3. Regional Heterogeneity in Wheat Yield Response to the CDHE

Although compound dry and hot events (CDHEs) have a widespread and significant negative impact on global wheat production, the magnitude of regional responses varies considerably (Lesk et al., 2022). At the global scale, major wheat-producing areas are generally exposed to CDHEs and are at high risk of negative yield anomalies. However, the sensitivity to CDHEs exhibits pronounced spatial heterogeneity across regions. This heterogeneity arises primarily from the interplay of multiple factors, including regional climatic conditions, water resource availability, agricultural management practices, and the physiological vulnerability of wheat crops (Hultgren et al., 2025).

Agricultural production in arid and semiarid regions (e.g., Central Asia, South Asia, and Eastern Europe) is predominantly rain-fed, making crops highly susceptible to the compounded effects of water stress and high temperatures (Zhang et al., 2024). Across the major Köppen climate zones, the multi-indicator results summarized in Figure S16 in Supporting Information S1 show that CDHE-related negative yield anomalies tend to be stronger in arid and semiarid regions than in humid or tropical regions, with temperate zones generally exhibiting intermediate responses across different drought–heat index combinations. These stresses are particularly pronounced during critical growth stages, especially heading and grain filling, when the synergy between drought and heat can lead to substantial reductions in the number of grains per spike and poor grain filling, ultimately resulting in severe negative yield anomalies (Mirosavljević et al., 2024; Qaseem et al., 2019). In contrast, regions with sufficient water resources or well-managed irrigation systems (e.g., China and parts of North America) are less vulnerable. The occurrence of CDHEs had less of an impact on changes in wheat yields than did areas with

little irrigation (Figure S17 in Supporting Information S1). Irrigation helps maintain soil moisture and reduce surface temperatures, thereby effectively alleviating the co-occurring stresses of drought and heat, and mitigating the negative impacts of CDHE on wheat yields (Li et al., 2020; Liu et al., 2024; Troy et al., 2015). However, the buffering role of irrigation needs to be viewed in the context of water-resource sustainability and potential trade-offs. More frequent CDHEs and warmer conditions are expected to increase irrigation water demand in many agricultural regions, particularly in basins that are already water-stressed, which may accelerate groundwater depletion and intensify competition with other water users (Lopez et al., 2022; Zhang et al., 2025). Under such conditions, shifting from water-intensive surface methods such as flood or furrow irrigation towards more efficient sprinkler or drip systems, together with improved irrigation scheduling, can help maintain wheat yields while slowing the growth in consumptive water use (Guo et al., 2022; Yang et al., 2020). Such adaptive measures are essential for enhancing the resilience of wheat production to increasing compound dry–hot stress under a warming climate.

Spring and winter wheat exhibit distinct sensitivities to CDHEs. To isolate phenological effects from regional climatic influences, we compared their CDHE exposure and yield responses within co-cultivated regions (Figure S18 in Supporting Information S1). Both spring and winter wheat show increasing CDHE proportions over 1982–2015, but the trend is steeper for spring wheat (1.4% decade^{-1}) than for winter wheat (0.7% decade^{-1}). Consistently, spring wheat shows a stronger negative correlation between CDHE frequency and yield anomalies ($r = -0.34, p < 0.05$) than winter wheat ($r = -0.26, p > 0.05$). This contrast is largely attributable to phenological timing: the critical reproductive stages of spring wheat often coincide with peak hot and dry conditions, when combined heat and water stress are known to cause large negative yield anomalies by damaging reproductive organs and limiting grain set and filling (Akter & Islam, 2017; Djanaguiraman et al., 2020). By contrast, winter wheat typically completes key developmental stages earlier in the season and is more frequently buffered by residual soil moisture and supplemental irrigation, which can sustain transpiration and reduce canopy and near-surface temperatures during warm, dry periods (Tack et al., 2017; Thiery et al., 2017). Together, these mechanisms help explain why spring wheat is more vulnerable to CDHEs than winter wheat in co-cultivated regions.

Moreover, the choice of drought–heat indicator combination plays a crucial role in accurately capturing crop responses (Feng et al., 2021; Li, Wang, Li, et al., 2025, Li, Wang, Li, et al., 2025). Compared with SPI-based combinations that rely solely on precipitation, combinations involving the SPEI or SSI generally exhibit stronger correlations with yield anomalies. This suggests that incorporating evapotranspiration demand or soil moisture dynamics into drought indices better reflects real crop water stress conditions, thereby improving the ability to explain yield variability (Chen et al., 2020; Yao et al., 2022). Similarly, temperature indicators such as the SSTI, which accounts for soil thermal conditions, are more effective in detecting prolonged heat episodes (García-García et al., 2023). These indices are better suited for capturing the long-term physiological stress imposed by sustained high temperatures, making them particularly valuable for precise assessments of yield loss risk under compound dry–hot conditions. Clarifying the mechanisms of these impact is essential for increasing the scientific accuracy and reliability of CDHE risk assessments. Clarifying these mechanisms and their interaction with irrigation conditions is essential for increasing the scientific accuracy and reliability of CDHE risk assessments and for designing region-specific, water-efficient adaptation strategies.

4.4. Limitations and Future Perspectives

Although this study provides a foundation for understanding the spatiotemporal characteristics of CDHEs in major global wheat-producing regions and its mechanisms of influence on yield, several issues where future research could enhance and extend the current findings remain.

First, the current analysis does not incorporate additional key physiological stress indicators, such as vapor pressure deficit (VPD), which has been shown in previous studies to more directly capture the effects of atmospheric dryness on crop physiological processes (Grossiord et al., 2020). Integrating the VPD and related parameters into the CDHE identification framework could increase the physiological relevance and explanatory power of dry–hot stress at the crop scale. Second, a unified absolute threshold was adopted to define CDHEs in this study. While this approach improves cross-regional comparability, it may overlook the variability in climate backgrounds and varietal sensitivity to heat and drought stress. Future research could explore percentile-based dynamic thresholds to improve the regional adaptability and agricultural applicability of these indicators (Wu, Hao, Tang, et al., 2020). Moreover, the use of annual yield data limits the ability to assess the stage-specific

impacts of CDHEs during critical periods of wheat growth. Future efforts should couple crop growth models (e.g., EPIC-IIASA) with high-resolution climate scenario data sets (e.g., CMIP6) to simulate how different types of CDHEs influence physiological processes and final yields at key developmental stages. Such an approach would enable a more detailed quantification of yield risks under future climate conditions (Jägermeyr, Müller, Ruane, et al., 2021). Furthermore, the potential benefits of different adaptation strategies (such as adjusting planting dates, optimizing irrigation methods, and breeding heat-tolerant and drought-resistant varieties) in mitigating the impacts of CDHEs must be assessed. A comprehensive quantitative framework based on models will provide scientific support for future agricultural climate risk management and policy-making. Future work could further disentangle externally forced signals from internal climate variability by combining longer observational records with large-ensemble climate simulations and explicit indices of major natural variability modes (e.g., PDO, AMO) when analyzing CDHE and yield time series.

5. Conclusion

In this study, the evolution of CDHE and their impacts on wheat yield across major global wheat-producing regions from 1981 to 2020 were assessed on the basis of multiple combinations of drought (SPI, SPEI, and SSI) and heat (STI and SSTI) indicators. Under continued global warming, the frequency, duration, and intensity of CDHEs during the wheat growing season have significantly increased, with the most pronounced trends observed in arid and semiarid regions such as Eastern Europe, Central Asia, and Turkey. These changes are closely linked to regional hydroclimatic conditions, coupled land–atmosphere processes, and agricultural management, with marked spatial heterogeneity.

The analysis revealed substantial differences among indicator combinations in identifying and characterizing CDHE trends. The SSI–SSTI combination, which incorporates soil characteristics, was the most sensitive to changes in frequency, whereas the SPEI–SSTI combination, which accounts for evapotranspiration demand, was most effective for assessing event intensity and duration. In contrast, the SPI–STI combination, which is based solely on precipitation and air temperature, tended to yield more conservative estimates in most regions. These findings underscore the importance of indicator selection for compound event detection and suggest that suitability assessments should integrate both meteorological–physiological mechanisms and regional environmental characteristics to increase stability and applicability. In this context, the SPEI–SSTI and SSI–SSTI combinations identified here provide process-oriented observational metrics that can be used to assess and improve the performance of current climate and Earth System Models (e.g., CMIP6) for simulating soil-moisture–temperature coupling and associated agricultural risks.

CDHEs have emerged as a significant threat to global wheat yields. When the percentage of CDHE days exceeded 10%, over 70% of the wheat-growing regions experienced negative yield anomalies, with an average reduction of 6.3%. However, yield responses varied considerably across regions, with Canada, Australia, and Central Asia exhibiting the highest vulnerability, whereas countries with extensive irrigation systems, such as China and India, presented more buffered impacts. Furthermore, combinations involving the SPEI or SSI as drought indicators and the SSTI as the heat indicator showed stronger correlations with negative yield anomalies across most major production regions. These results highlight the advantages of incorporating evapotranspiration and soil moisture status to more accurately capture crop stress under compound extremes. This study clarifies the evolving characteristics and agricultural risks of CDHEs and provides a scientific foundation for developing region-specific adaptation strategies and agricultural management policies in the context of increasing climate extremes, emphasizing the importance of appropriate monitoring indicators and region-specific adaptation planning to enhance agricultural resilience. By integrating multiple drought and heat indices within a multi-indicator assessment framework and identifying combinations that better capture key stress signals across regions and growth stages, this study can help optimize agrometeorological monitoring and early-warning systems for CDHE risk. It also provides decision-relevant evidence for regionally adaptive cropping systems (e.g., stress-tolerant cultivar selection and planting date adjustments). Furthermore, it can support irrigation planning and water allocation decisions, and may inform broader water-management policies under intensifying compound extremes.

Conflict of Interest

The authors declare no conflicts of interest relevant to this study.

Availability Statement

All data used in this study are publicly available. Daily climate reanalysis data used to construct CDHE indices were obtained from the ERA5 post-processed daily-statistics on single levels product of the Copernicus Climate Change Service Climate Data Store, (2024). Gridded wheat yield data were primarily taken from the Global Data set of Historical Yields for Major Crops (GDHY; Iizumi, 2019), with additional coverage from the Global-CropYield5min data set (Cao et al., 2024) to improve spatial completeness. Global wheat harvested area, crop calendar information, and crop type classification data were derived from SPAM2010 (IFPRI, 2019), the GGCMI Phase 3 crop calendar data set (Jägermeyr, Müller, Minoli, et al., 2021), and the GEOGLAM global crop mask (Becker-Reshef et al., 2022). All data sets are summarized in Table S1 in Supporting Information S1. Some sources may require user registration prior to data access.

Acknowledgments
This work was supported by Foundation: the Key Research Program of the National Natural Science Foundation of China (Grant 42330502); and the National Key Research and Development Program-Global Change and Mitigation Project (Grant 2016YFA0602404).

References

Afrooz, M. D., Chen, G., & Anandhi, A. (2023). Drought- and heatwave-associated compound extremes: A review of hotspots, variables, parameters, drivers, impacts, and analysis frameworks. *Frontiers in Earth Science*, *10*, 914437. https://doi.org/10.3389/feart.2022.914437

Agrafiotis, D. (2014). Video error concealment. In D. R. Bull (Ed.), *Academic press library in signal processing: Image and video compression and multimedia* (Vol. 5, pp. 295–321). Elsevier. https://doi.org/10.1016/B978-0-12-420149-1.00009-0

Akter, N., & Islam, M. R. (2017). Heat stress effects and management in wheat: A review. *Agronomy for Sustainable Development*, *37*(37). https://doi.org/10.1007/s13593-017-0443-9

Becker-Reshef, I., Barker, B., Whitcraft, A., Oliva, P., Mobley, K., Justice, C., & Sahajpal, R. (2022). GEOGLAM best available crop type masks (1.0.0) [Dataset]. *Zenodo*. https://doi.org/10.5281/zenodo.7230863

Benjamini, Y., & Hochberg, Y. (1995). Controlling the false discovery rate: A practical and powerful approach to multiple testing. *Journal of the Royal Statistical Society: Series B*, *57*(1), 289–300. https://doi.org/10.1111/j.2517-6161.1995.tb02031.x

Bevacqua, E., Zappa, G., Lehner, F., & Zscheischler, J. (2022). Precipitation trends determine future occurrences of compound hot-dry events. *Nature Climate Change*, *12*(4), 350–355. https://doi.org/10.1038/s41558-022-01309-5

Cao, J., Zhang, Z., Luo, X., Luo, Y., Xu, J., Xie, J., et al. (2025). Mapping global yields of four major crops at 5-minute resolution from 1982 to 2015 using multi-source data and machine learning. *Scientific Data*, *12*(1), 357. https://doi.org/10.1038/s41597-025-04650-4

Cao, J., Zhang, Z., Luo, X., Xu, J., Luo, Y., Xie, J., et al. (2024). GlobalCropYield5min: A global gridded annual major crops yield dataset at 5-minute resolution during 1982–2015 [Dataset]. *Mendeley Data*, *V3*. https://doi.org/10.17632/hg8wzgx4yp.3

Chen, H., & Wang, S. (2023). Compound dry and wet extremes lead to an increased risk of rice yield loss. *Geophysical Research Letters*, *50*(24), e2023GL105817. https://doi.org/10.1029/2023GL105817

Chen, X., Li, Y., Yao, N., Liu, D. L., Javed, T., Liu, C., & Liu, F. (2020). Impacts of multi-timescale SPEI and SMDI variations on winter wheat yields. *Agricultural Systems*, *185*, 102955. https://doi.org/10.1016/j.agsy.2020.102955

Cohen, I., Zandalinas, S. I., Huck, C., Fritschi, F. B., & Mittler, R. (2021). Meta-analysis of drought and heat stress combination impact on crop yield and yield components. *Physiologia Plantarum*, *171*(1), 66–76. https://doi.org/10.1111/ppl.13203

Copernicus Climate Change Service Climate, D. S. (2024). ERA5 post-processed daily-statistics on single levels from 1940 to present [Dataset]. *Copernicus Climate Change Service (C3S) Climate Data Store (CDS)*. https://doi.org/10.24381/cds.4991cf48

Djanaguiraman, M., Narayanan, S., Erdayani, E., & Prasad, P. V. V. (2020). Effects of high temperature stress during anthesis and grain filling periods on photosynthesis, lipids and grain yield in wheat. *BMC Plant Biology*, *20*(268), 268. https://doi.org/10.1186/s12870-020-02479-0

Dracup, J. A., Lee, K. S., & Paulson, E. J., Jr. (1980). On the definition of droughts. *Water Resources Research*, *16*(2), 297–302. https://doi.org/10.1029/WR016i002p00297

Droogers, P., & Allen, R. G. (2002). Estimating reference evapotranspiration under inaccurate data conditions. *Irrigation and Drainage Systems*, *16*(1), 33–45. https://doi.org/10.1023/A:1015508322413

Fahad, S., Bajwa, A. A., Nazir, U., Anjum, S. A., Farooq, A., Zohaib, A., et al. (2017). Crop production under drought and heat stress: Plant responses and management options. *Frontiers in Plant Science*, *8*, 1147. https://doi.org/10.3389/fpls.2017.01147

Fan, X., Zhang, Y., Shi, K., Peng, J., Liu, Y., Zhou, Y., et al. (2024). Surging compound drought-heatwaves underrated in global soils. *Proceedings of the National Academy of Sciences*, *121*(42), e2410294121. https://doi.org/10.1073/pnas.2410294121

Feng, S., Hao, Z., Wu, X., Zhang, X., & Hao, F. (2021). A multi-index evaluation of changes in compound dry and hot events of global maize areas. *Journal of Hydrology*, *602*, 126728. https://doi.org/10.1016/j.jhydrol.2021.126728

Friedman, M. (1937). The use of ranks to avoid the assumption of normality implicit in the analysis of variance. *Journal of the American Statistical Association*, *32*(200), 675–701. https://doi.org/10.1080/01621459.1937.10503522

García-García, A., Cuesta-Valero, F. J., Miralles, D. G., Mahecha, M. D., Quaas, J., Reichstein, M., et al. (2023). Soil heat extremes can outpace air temperature extremes. *Nature Climate Change*, *13*(11), 1237–1241. https://doi.org/10.1038/s41558-023-01812-3

Gebrechorkos, S. H., Sheffield, J., Vicente-Serrano, S. M., Funk, C., Miralles, D. G., Peng, J., et al. (2025). Warming accelerates global drought severity. *Nature*, *642*(8068), 628–635. https://doi.org/10.1038/s41586-025-09047-2

Geirinhas, J. L., Russo, A., Libonati, R., Sousa, P. M., Miralles, D. G., & Trigo, R. M. (2021). Recent increasing frequency of compound summer drought and heatwaves in southeast Brazil. *Environmental Research Letters*, *16*(3), 034036. https://doi.org/10.1088/1748-9326/abe0eb

Goulart, H. M. D., Van der Wiel, K., Folberth, C., Balkovic, J., & Van den Hurk, B. J. J. M. (2021). Storylines of weather-induced crop failure events under climate change. *Earth System Dynamics*, *12*(4), 1503–1527. https://doi.org/10.5194/esd-12-1503-2021

Gringorten, I. I. (1963). A plotting rule for extreme probability paper. *Journal of Geophysical Research*, *68*(3), 813–814. https://doi.org/10.1029/JZ068i003p00813

Grossiord, C., Buckley, T. N., Cernusak, L. A., Novick, K. A., Poulter, B., Siegwolf, R. T. W., et al. (2020). Plant responses to rising vapor pressure deficit. *New Phytologist*, *226*(6), 1550–1566. https://doi.org/10.1111/nph.16485

Gu, L., Chen, J., Yin, J., Slater, L. J., Wang, H. M., Guo, Q., et al. (2022). Global increases in compound flood-hot extreme hazards under climate warming. *Geophysical Research Letters*, *49*(8), e2022GL097726. https://doi.org/10.1029/2022GL097726

Guo, X., Zhao, Q., Li, J., Wang, Z., Zhang, Y., & Xue, X. (2022). Daily drip irrigation based on real-time weather improves winter wheat grain yield and water use efficiency. *Irrigation and Drainage*, *71*(3), 589–603. https://doi.org/10.1002/ird.2673

Hamed, R., van Loon, A. F., Aerts, J. C. J. H., & Coumou, D. (2021). Impacts of compound hot-dry extremes on US soybean yields. *Earth System Dynamics*, *12*(4), 1371–1391. https://doi.org/10.5194/esd-12-1371-2021

Hao, Z., & Chen, Y. (2024). Research progresses and prospects of multi-sphere compound extremes from the Earth system perspective. *Science China Earth Sciences*, *67*(2), 343–374. https://doi.org/10.1007/s11430-023-1201-y

Hao, Z., Hao, F., Singh, V. P., & Zhang, X. (2018). Changes in the severity of compound drought and hot extremes over global land areas. *Environmental Research Letters*, *13*(12), 124022. https://doi.org/10.1088/1748-9326/aaee96

Hao, Z., Hao, F., Xia, Y., Feng, S., Sun, C., Zhang, X., et al. (2022). Compound droughts and hot extremes: Characteristics, drivers, changes, and impacts. *Earth-Science Reviews*, *235*, 104241. https://doi.org/10.1016/j.earscirev.2022.104241

He, Y., Fang, J., Xu, W., & Shi, P. (2022). Substantial increase of compound droughts and heatwaves in wheat growing seasons worldwide. *International Journal of Climatology*, *42*(10), 5038–5054. https://doi.org/10.1002/joc.7518

He, Y., Zhao, Y., Sun, S., Fang, J., Zhang, Y., Sun, Q., et al. (2024). Global warming determines future increase in compound dry and hot days within wheat growing seasons worldwide. *Climatic Change*, *177*(4), 70. https://doi.org/10.1007/s10584-024-03718-1

Heino, M., Kinnunen, P., Anderson, W., Ray, D. K., Puma, M. J., Varis, O., et al. (2023). Increased probability of hot and dry weather extremes during the growing season threatens global crop yields. *Scientific Reports*, *13*(1), 3583. Article 3583. https://doi.org/10.1038/s41598-023-29378-2

Hersbach, H., Comyn-Platt, E., Bell, B., Berrisford, P., Biavati, G., Horányi, A., et al. (2023). ERA5 post-processed daily statistics on pressure levels from 1940 to present. Copernicus Climate data Store (CDS). https://doi.org/10.24381/cds.50314f4c

Hosseinzadehtalaei, P., Termonia, P., & Tabari, H. (2024). Projected changes in compound hot-dry events depend on the dry indicator considered. *Communications Earth and Environment*, *5*(1), 220. https://doi.org/10.1038/s43247-024-01352-4

Hu, Y., Wang, W., Wang, P., Teuling, A. J., & Zhu, Y. (2024). Spatial-temporal variations and drivers of the compound dry-hot event in China. *Atmospheric Research*, *299*, 107160. https://doi.org/10.1016/j.atmosres.2023.107160

Hultgren, A., Carleton, T. A., Delgado, M., Gergel, D. R., Greenstone, M., Houser, T., et al. (2025). Impacts of climate change on global agriculture accounting for adaptation. *Nature*, *642*(8068), 644–652. https://doi.org/10.1038/s41586-025-09085-w

Iizumi, T. (2019). Global dataset of historical yields v1.2 and v1.3 aligned version [Dataset]. *PANGAEA*. https://doi.org/10.1594/PANGAEA.909132

Iizumi, T., & Sakai, T. (2020). The global dataset of historical yields for major crops 1981-2016. *Scientific Data*, *7*(1), 1–7. https://doi.org/10.1038/s41597-020-0433-7

International Food Policy Research Institute (IFPRI). (2019). Global spatially-disaggregated crop production statistics data for 2010, version 2.0 (SPAM2010) [Dataset]. *Harvard Dataverse*, *V4*. https://doi.org/10.7910/DVN/PRFF8V

IPCC. (2021). *Climate change 2021: The physical science basis. Contribution of working group I to the sixth assessment report of the intergovernmental panel on climate change*. Cambridge University Press. Retrieved from https://www.ipcc.ch/report/ar6/wg1/

Jägermeyr, J., Müller, C., Minoli, S., Ray, D., & Siebert, S. (2021). GGCMI phase 3 crop calendar [Dataset]. *Zenodo*. https://doi.org/10.5281/zenodo.5062513

Jägermeyr, J., Müller, C., Ruane, A. C., Elliott, J., Balkovic, J., Castillo, O., et al. (2021). Climate impacts on global agriculture emerge earlier in new generation of climate and crop models. *Nature Food*, *2*(11), 873–885. https://doi.org/10.1038/s43016-021-00400-y

Jiang, L., Zhang, J., Bai, L., Han, J., Meng, X., Cao, D., & Al-Sakkaf, A. S. (2025). Increased frequency and severity of global compound dry and heat wave events in a daily scale. *Journal of Hydrology*, *654*, 132857. https://doi.org/10.1016/j.jhydrol.2025.132857

Jiang, T., He, L., Feng, H., He, J., & Yu, Q. (2025). Understanding the impacts of extreme temperature and humidity compounds on winter wheat traits in China. *Agricultural and Forest Meteorology*, *362*, 110354. https://doi.org/10.1016/j.agrformet.2024.110354

Lesk, C., & Anderson, W. (2021). Decadal variability modulates trends in concurrent heat and drought over global croplands. *Environmental Research Letters*, *16*(5), 055024. https://doi.org/10.1088/1748-9326/abeb35

Lesk, C., Anderson, W., Rigden, A., Coast, O., Jägermeyr, J., McDermid, S., et al. (2022). Compound heat and moisture extreme impacts on global crop yields under climate change. *Nature Reviews Earth and Environment*, *3*(12), 872–889. https://doi.org/10.1038/s43017-022-00368-8

Lesk, C., Rowhani, P., & Ramankutty, N. (2016). Influence of extreme weather disasters on global crop production. *Nature*, *529*(7584), 84–87. https://doi.org/10.1038/nature16467

Li, Q., Wang, P., Li, Y., Tang, J., Li, X., Zhang, Y., et al. (2025). Hazard assessment of compound drought and heat events on summer maize from agricultural and meteorological perspectives. *Agricultural Water Management*, *313*, 109479. https://doi.org/10.1016/j.agwat.2025.109479

Li, S., Wang, B., Liu, D. L., Chen, C., Feng, P., Huete, A., et al. (2025). The contribution of climate drivers to compound drought and extreme temperature events increased in recent decades. *Weather and Climate Extremes*, *49*, 100793. https://doi.org/10.1016/j.wace.2025.100793

Li, Y., Guan, K., Peng, B., Franz, T. E., Wardlow, B., & Pan, M. (2020). Quantifying irrigation cooling benefits to maize yield in the US midwest. *Global Change Biology*, *26*(5), 3065–3078. https://doi.org/10.1111/gcb.15002

Lin, J., & Qian, T. (2022). The Atlantic multi-decadal oscillation. *Atmosphere-Ocean*, *60*(3–4), 307–337. https://doi.org/10.1080/07055900.2022.2085876

Liu, H., Ren, Y., Zhou, X., & Liu, R. (2024). Mitigating dry-hot-windy climate disasters in wheat fields using the sprinkler irrigation method. *Agronomy*, *14*(9), 1962. https://doi.org/10.3390/agronomy14091962

Liu, M., & Sun, A. Y. (2020). A physical agricultural drought index based on root zone water availability: Model development and application. *Geophysical Research Letters*, *47*(22), e2020GL088553. https://doi.org/10.1029/2020GL088553

Liu, W., Li, Z., Li, Y., Ye, T., Chen, S., & Liu, Y. (2022). Heterogeneous impacts of excessive wetness on maize yields in China: Evidence from statistical yields and process-based crop models. *Agricultural and Forest Meteorology*, *327*, 109205. https://doi.org/10.1016/j.agrformet.2022.109205

Liu, Z., Jiao, L., & Lian, X. (2025). Changes in compound extreme events and their impacts on cropland productivity in China, 1985-2019. *Earth's Future*, *13*(3), e2024EF005038. https://doi.org/10.1029/2024EF005038

Lopez, J. R., Winter, J. M., Elliott, J., Ruane, A. C., Porter, C., Hoogenboom, G., et al. (2022). Sustainable use of groundwater May dramatically reduce irrigated production of maize, soybean, and wheat. *Earth's Future*, *10*(1), e2021EF002018. https://doi.org/10.1029/2021EF002018

Ma, Q., Hao, Z., Zhang, Y., & Pang, Y. (2025). Likelihoods of compound dry-hot-windy events are projected to increase under global warming. *Atmospheric Research*, *322*, 108119. https://doi.org/10.1016/j.atmosres.2025.108119

Markonis, Y., Kumar, R., Hanel, M., Rakovec, O., Máca, P., AghaKouchak, A., et al. (2021). The rise of compound warm-season droughts in Europe. *Science Advances*, *7*(6), eabb9668. https://doi.org/10.1126/sciadv.abb9668

McKinnon, K. A., & Deser, C. (2018). Internal variability and regional climate trends in an observational large ensemble. *Journal of Climate*, *31*(17), 6783–6802. https://doi.org/10.1175/JCLI-D-17-0901.1

Mirosavljević, M., Mikić, S., Župunski, V., Abdelhakim, L., Trkulja, D., Zhou, R., et al. (2024). Effects of heat stress during anthesis and grain filling stages on some physiological and agronomic traits in diverse wheat genotypes. *Plants*, *13*(15), 2083. https://doi.org/10.3390/plants13152083

Moradian, S., Gharbia, S., AghaKouchak, A., Torabi Haghighi, A., & Olbert, A. I. (2025). Integrated multi-index drought monitoring and projection under climate change. *Atmospheric Research*, *316*, 107946. https://doi.org/10.1016/j.atmosres.2025.107946

Mukherjee, S., & Mishra, A. K. (2021). Increase in compound drought and heatwaves in a warming world. *Geophysical Research Letters*, *48*(1), e2020GL090617. https://doi.org/10.1029/2020GL090617

Mukherjee, S., Mishra, A. K., Zscheischler, J., & Entekhabi, D. (2023). Interaction between dry and hot extremes at a global scale using a Cascade modeling framework. *Nature Communications*, *14*(1), 277. https://doi.org/10.1038/s41467-022-35748-7

Müller, C., Elliott, J., Chryssanthacopoulos, J., Arneth, A., Balkovic, J., Ciais, P., et al. (2017). Global gridded crop model evaluation: Benchmarking, skills, deficiencies and implications. *Geoscientific Model Development*, *10*(4), 1403–1422. https://doi.org/10.5194/gmd-10-1403-2017

Newman, M., Alexander, M. A., Ault, T. R., Cobb, K. M., Deser, C., Di Lorenzo, E., et al. (2016). The Pacific decadal oscillation, revisited. *Journal of Climate*, *29*(12), 4399–4427. https://doi.org/10.1175/JCLI-D-15-0508.1

Pearson, K. (1895). Contributions to the mathematical theory of evolution. II. Skew variation in homogeneous material. *Philosophical Transactions of the Royal Society of London A*, *186*, 343–414. https://doi.org/10.1098/rsta.1895.0010

Peng, L., Sheffield, J., Wei, Z., Ek, M., & Wood, E. F. (2024). An enhanced standardized precipitation-evapotranspiration index (SPEI) drought-monitoring method integrating land-surface characteristics. *Earth System Dynamics*, *15*(5), 1277–1300. https://doi.org/10.5194/esd-15-1277-2024

Prabhakar, A., Mitra, S., & Varghese, F. C. (2023). Multi-index characterization of compound dry-hot events in India. *International Journal of Climatology*, *43*(13), 6243–6267. https://doi.org/10.1002/joc.8203

Qaseem, M. F., Qureshi, R., & Shaheen, H. (2019). Effects of pre-anthesis drought, heat and their combination on the growth, yield and physiology of diverse wheat (Triticum aestivum L.) genotypes varying in sensitivity to heat and drought stress. *Scientific Reports*, *9*(1), 6955. https://doi.org/10.1038/s41598-019-43477-z

Rajeev, A., Mahto, S. S., & Mishra, V. (2022). Climate warming and summer monsoon breaks drive compound dry and hot extremes in India. *iScience*, *25*(11), 105377. https://doi.org/10.1016/j.isci.2022.105377

Rezaei, E. E., Webber, H., Asseng, S., Boote, K. J., Durand, J. L., Ewert, F., et al. (2023). Climate change impacts on crop yields. *Nature Reviews Earth and Environment*, *4*(12), 831–846. https://doi.org/10.1038/s43017-023-00491-0

Shan, B., Verhoest, N. E. C., & De Baets, B. (2024). Identification of compound drought and heatwave events on a daily scale and across four seasons. *Hydrology and Earth System Sciences*, *28*(9), 2065–2080. https://doi.org/10.5194/hess-28-2065-2024

Stagge, J. H., Tallaksen, L. M., Gudmundsson, L., van Loon, A. F., & Stahl, K. (2015). Candidate distributions for climatological drought indices (SPI and SPEI). *International Journal of Climatology*, *35*(13), 4027–4040. https://doi.org/10.1002/joc.4267

Tack, J., Barkley, A., & Hendricks, N. (2017). Irrigation offsets wheat yield reductions from warming temperatures. *Environmental Research Letters*, *12*(11), 114027. https://doi.org/10.1088/1748-9326/aa8d27

Thiery, W., Davin, E. L., Lawrence, D. M., Hirsch, A. L., Hauser, M., & Seneviratne, S. I. (2017). Present-day irrigation mitigates heat extremes. *Journal of Geophysical Research: Atmospheres*, *122*(3), 1403–1422. https://doi.org/10.1002/2016JD025740

Toreti, A., Cronie, O., & Zampieri, M. (2019). Concurrent climate extremes in the key wheat producing regions of the world. *Scientific Reports*, *9*(1), 5493. https://doi.org/10.1038/s41598-019-41932-5

Tricker, P. J., ElHabti, A., Schmidt, J., & Fleury, D. (2018). The physiological and genetic basis of combined drought and heat tolerance in wheat. *Journal of Experimental Botany*, *69*(13), 3195–3210. https://doi.org/10.1093/jxb/ery081

Tripathy, K. P., Mukherjee, S., Mishra, A. K., Mann, M. E., & Williams, A. P. (2023). Climate change will accelerate the high-end risk of compound drought and heatwave events. *Proceedings of the National Academy of Sciences of the United States of America*, *120*(28), e2219825120. https://doi.org/10.1073/pnas.2219825120

Troy, T. J., Kipgen, C., & Pal, I. (2015). The impact of climate extremes and irrigation on US crop yields. *Environmental Research Letters*, *10*(5), 054013. https://doi.org/10.1088/1748-9326/10/5/054013

Vicente-Serrano, S. M., Beguería, S., & López-Moreno, J. I. (2010). A multiscalar drought index sensitive to global warming: The standardized precipitation evapotranspiration index. *Journal of Climate*, *23*(7), 1696–1718. https://doi.org/10.1175/2009JCLI2909.1

Wang, H., Zhang, G., Zhang, S., Shi, L., Su, X., Song, S., et al. (2023). Development of a novel daily-scale compound dry and hot index and its application across seven climatic regions of China. *Atmospheric Research*, *287*, 106700. https://doi.org/10.1016/j.atmosres.2023.106700

Wang, Q., Zeng, J., Qi, J., Zhang, X., Zeng, Y., Shui, W., et al. (2021). A multi-scale daily SPEI dataset for drought characterization at observation stations over mainland China from 1961 to 2018. *Earth System Science Data*, *13*(2), 331–341. https://doi.org/10.5194/essd-13-331-2021

Wu, H., Su, X., Singh, V. P., Feng, K., & Niu, J. (2021). Agricultural drought prediction based on conditional distributions of Vine copulas. *Water Resources Research*, *57*(8), e2021WR029562. https://doi.org/10.1029/2021WR029562

Wu, X., Hao, Z., Hao, F., Singh, V. P., & Zhang, X. (2019). Dry-hot magnitude index: A joint indicator for compound event analysis. *Environmental Research Letters*, *14*(6), 064017. https://doi.org/10.1088/1748-9326/ab1ec7

Wu, X., Hao, Z., Tang, Q., Singh, V. P., Zhang, X., & Hao, F. (2020). Projected increase in compound dry and hot events over global land areas. *International Journal of Climatology*, *41*(3), 393–403. https://doi.org/10.1002/joc.6626

Wu, X., Hao, Z., Zhang, X., Li, C., & Hao, F. (2020). Evaluation of severity changes of compound dry and hot events in China based on a multivariate multi-index approach. *Journal of Hydrology*, *583*, 124580. https://doi.org/10.1016/j.jhydrol.2020.124580

Yang, J., Wu, J., Zhou, L., Zhou, H., Zhang, Z., & Zhang, R. (2025). Characteristics of compound heat and drought events during the spring maize growing season in northeast China based on a novel daily-scale analysis framework. *Journal of Hydrology: Regional Studies*, *57*, 102140. https://doi.org/10.1016/j.ejrh.2024.102140

Yang, M., Leghari, S. J., Guan, X., Ma, S., Ding, C., Mei, F., et al. (2020). Deficit subsurface drip irrigation improves water use efficiency and stabilizes yield by enhancing subsoil water extraction in winter wheat. *Frontiers in Plant Science*, *11*, 508. https://doi.org/10.3389/fpls.2020.00508

Yao, N., Li, Y., Liu, Q., Zhang, S., Chen, X., Ji, Y., et al. (2022). Response of wheat and maize growth-yields to meteorological and agricultural droughts based on standardized precipitation evapotranspiration indexes and soil moisture deficit indexes. *Agricultural Water Management*, *266*, 107566. https://doi.org/10.1016/j.agwat.2022.107566

Ye, T., Nie, J., Wang, J., Shi, P., & Wang, Z. (2015). Performance of detrending models of crop yield risk assessment: Evaluation on real and hypothetical yield data. *Stochastic Environmental Research and Risk Assessment*, *29*(1), 109–117. https://doi.org/10.1007/s00477-014-0871-x

Yin, J., & Slater, L. (2023). Understanding heatwave-drought compound hazards and impacts on socio-ecosystems. *The Innovation Geoscience*, *1*(3), 100042. https://doi.org/10.59717/j.xinn-geo.2023.100042

Yu, Q., You, L., Wood-Sichra, U., Ru, Y., Joglekar, A. K. B., Fritz, S., et al. (2020). A cultivated planet in 2010 - Part 2: The global gridded agricultural-production maps. *Earth System Science Data*, *12*(4), 3545–3572. https://doi.org/10.5194/essd-12-3545-2020

Zampieri, M., Ceglar, A., Dentener, F., & Toreti, A. (2017). Wheat yield loss attributable to heat waves, drought, and water excess at the global, national, and subnational scales. *Environmental Research Letters*, *12*(6), 064008. https://doi.org/10.1088/1748-9326/aa723b

Zeng, Z., Wu, W., Peñuelas, J., Li, Y., Jiao, W., Li, Z., et al. (2023). Increased risk of flash droughts with raised concurrent hot and dry extremes under global warming. *npj Climate and Atmospheric Science*, *6*(1), 134. https://doi.org/10.1038/s41612-023-00468-2

Zhang, G., Zhang, S., Wang, H., Gan, T. Y., Su, X., Wu, H., et al. (2024). Evaluating vegetation vulnerability under compound dry and hot conditions using Vine copula across global lands. *Journal of Hydrology*, *631*, 130775. https://doi.org/10.1016/j.jhydrol.2024.130775

Zhang, W., Zhao, X., Gao, X., Liang, W., Li, J., & Zhang, B. (2025). Spatially explicit assessment of water stress and potential mitigating solutions in a large water-limited basin: The yellow river basin in China. *Hydrology and Earth System Sciences*, *29*(2), 507–524. https://doi.org/10.5194/hess-29-507-2025

Zhang, Y., Hao, Z., Jiang, Y., & Singh, V. P. (2023a). Global warming increases risk from compound dry hot events to human and agricultural systems. *International Journal of Climatology*, *43*(14), 6706–6719. https://doi.org/10.1002/joc.8229

Zhang, Y., Hao, Z., Jiang, Y., & Singh, V. P. (2023b). Impact-based evaluation of multivariate drought indicators for drought monitoring in China. *Global and Planetary Change*, *228*, 104219. https://doi.org/10.1016/j.gloplacha.2023.104219

Zhao, H., Zhang, L., Kirkham, M. B., Welch, S. M., Nielsen-Gammon, J. W., Bai, G., et al. (2022). U.S. winter wheat yield loss attributed to compound hot-dry-windy events. *Nature Communications*, *13*(1), 7233. https://doi.org/10.1038/s41467-022-34947-6

Zscheischler, J., & Seneviratne, S. I. (2017). Dependence of drivers affects risks associated with compound events. *Science Advances*, *3*(6), e1700263. https://doi.org/10.1126/sciadv.1700263

Zscheischler, J., Westra, S., Van den Hurk, B. J. J. M., Seneviratne, S. I., Ward, P. J., Pitman, A., et al. (2018). Future climate risk from compound events. *Nature Climate Change*, *8*(6), 469–477. https://doi.org/10.1038/s41558-018-0156-3

References From the Supporting Information

Hao, Z., Hao, F., Singh, V. P., Xia, Y., Shi, C., & Zhang, X. (2018). A multivariate approach for statistical assessments of compound extremes. *Journal of Hydrology*, *565*, 87–94. https://doi.org/10.1016/j.jhydrol.2018.08.025

Li, J., Wang, Z., Wu, X., Xu, C.-Y., Guo, S., & Chen, X. (2020). Toward monitoring short-term droughts using a novel daily scale, standardized antecedent precipitation evapotranspiration index. *Journal of Hydrometeorology*, *21*(5), 891–908. https://doi.org/10.1175/JHM-D-19-0298.1

Zscheischler, J., Michalak, A. M., Schwalm, C., Mahecha, M. D., Huntzinger, D. N., Reichstein, M., et al. (2014). Impact of large-scale climate extremes on biospheric carbon fluxes: An intercomparison based on MsTMIP data. *Global Biogeochemical Cycles*, *28*(6), 585–600. https://doi.org/10.1002/2014GB004826